Human Metastatic Cholangiocarcinoma Patient-Derived Xenografts and Tumoroids for Preclinical Drug Evaluation

Queralt Serra-Camprubí[1], Helena Verdaguer[1,2], Winona Oliveros[3], Núria Lupión-Garcia[1], Alba Llop-Guevara[1], Cristina Molina[1], Maria Vila-Casadesús[4], Anthony Turpin[5,6], Cindy Neuzillet[7], Joan Frigola[8], Jessica Querol[1], Mariana Yáñez-Bartolomé[1], Florian Castet[1,2], Carles Fabregat-Franco[1,2], Carmen Escudero-Iriarte[1], Marta Escorihuela[1], Enrique J. Arenas[1], Cristina Bernadó-Morales[1], Noemí Haro[9], Francis J. Giles[10], Óscar J. Pozo[9], Josep M. Miquel[1], Paolo G. Nuciforo[1], Ana Vivancos[4], Marta Melé[3], Violeta Serra[1], Joaquín Arribas[1,11,12,13,14], Josep Tabernero[1,2], Sandra Peiró[1], Teresa Macarulla[1,2], and Tian V. Tian[1]

ABSTRACT

Purpose: Cholangiocarcinoma (CCA) is usually diagnosed at advanced stages, with limited therapeutic options. Preclinical models focused on unresectable metastatic CCA are necessary to develop rational treatments. Pathogenic mutations in *IDH1/2*, *ARID1A/B*, *BAP1*, and *BRCA1/2* have been identified in 30%–50% of patients with CCA. Several types of tumor cells harboring these mutations exhibit homologous recombination deficiency (HRD) phenotype with enhanced sensitivity to PARP inhibitors (PARPi). However, PARPi treatment has not yet been tested for effectiveness in patient-derived models of advanced CCA.

Experimental Design: We have established a collection of patient-derived xenografts from patients with unresectable metastatic CCA (CCA_PDX). The CCA_PDXs were characterized at both histopathologic and genomic levels. We optimized a protocol to generate CCA tumoroids from CCA_PDXs. We tested the effects of PARPis in both CCA tumoroids and CCA_PDXs. Finally, we used the RAD51 assay to evaluate the HRD status of CCA tissues.

Results: This collection of CCA_PDXs recapitulates the histopathologic and molecular features of their original tumors. PARPi treatments inhibited the growth of CCA tumoroids and CCA_PDXs with pathogenic mutations of *BRCA2*, but not those with mutations of *IDH1*, *ARID1A*, or *BAP1*. In line with these findings, only CCA_PDX and CCA patient biopsy samples with mutations of *BRCA2* showed RAD51 scores compatible with HRD.

Conclusions: Our results suggest that patients with advanced CCA with pathogenic mutations of *BRCA2*, but not those with mutations of *IDH1*, *ARID1A*, or *BAP1*, are likely to benefit from PARPi therapy. This collection of CCA_PDXs provides new opportunities for evaluating drug response and prioritizing clinical trials.

Introduction

Cholangiocarcinomas (CCA) are a diverse group of malignancies of the biliary tract (1). After hepatocellular carcinoma (HCC), CCA is the second most common primary hepatic malignancy (2). Often asymptomatic at early stages, CCA is usually diagnosed at an advanced stage with limited therapeutic options (2). This lack of efficient treatment for patients with advanced CCA is associated with a dismal prognosis: the 5-year survival rate of patients with advanced metastatic CCA is only 2% (3). Thus, there is an urgent need to develop efficient treatments for patients with advanced CCA.

Patient-derived xenografts (PDX) are generated by transplanting intact and surgically derived tumor samples from patients into mice. PDX models retain the characteristics of tumors from distinct patients and recapitulate intratumor and intertumor heterogeneity (4, 5). Importantly, PDX models exhibit treatment responses

[1]Preclinical and Translational Research Program, Vall d'Hebron Institute of Oncology (VHIO), Barcelona, Spain. [2]Gastrointestinal and Endocrine Tumor Unit, Vall d'Hebron Institute of Oncology (VHIO), Hospital Universitari Vall d'Hebron, Vall d'Hebron Barcelona Hospital Campus, Barcelona, Spain. [3]Life Sciences Department, Barcelona Supercomputing Center (BSC), Barcelona, Spain. [4]Cancer Genomics Group, Vall d'Hebron Institute of Oncology (VHIO), Barcelona, Spain. [5]Université de Lille, CNRS INSERM UMR9020-U1277, CANTHER Cancer Heterogeneity Plasticity and Resistance to Therapies, Lille, France. [6]Medical Oncology Department, CHRU Lille, Lille, France. [7]Gastrointestinal Oncology, Medical Oncology Department, Curie Institute, Versailles St-Quentin-Paris Saclay University, Saint-Cloud, France. [8]Clinical Research Program, Vall d'Hebron Institute of Oncology (VHIO), Barcelona, Spain. [9]Neurosciences Research Program, IMIM (Hospital del Mar Medical Research Institute), Barcelona, Spain. [10]Developmental Therapeutics Consortium, Chicago, Illinois. [11]Centro de Investigación Biomédica en Red de Cáncer, Monforte de Lemos, Madrid, Spain. [12]Department of Medicine and Life Sciences, Universitat Pompeu Fabra (UPF), Barcelona, Spain. [13]Cancer Research Program, IMIM (Hospital del Mar Medical Research Institute), Barcelona, Spain. [14]Institució Catalana de Recerca i Estudis Avançats (ICREA), Barcelona, Spain.

S. Peiró, T. Macarulla, and T.V. Tian contributed equally to this article.

Corresponding Authors: Tian V. Tian, Vall d'Hebron Institute of Oncology (VHIO), Barcelona 08035, Spain. Phone: (34)932543450, ext. 8656; E-mail: tiantian@vhio.net; Teresa Macarulla, tmacarulla@vhio.net; and Sandra Peiró, speiro@vhio.net

Translational Relevance

Currently, only limited therapeutic options are available for patients with unresectable advanced cholangiocarcinoma (CCA). Preclinical models focused on unresectable metastatic CCA are necessary to develop rational treatments. We present a unique collection of patient-derived xenografts from patients with CCA with unresectable metastatic diseases (CCA_PDX). Using these preclinical models, we identified that pathogenic mutations of *BRCA2*, but not those of *IDH1*, *ARID1A*, or *BAP1*, were associated with the sensitivity to PARP inhibitor (PARPi) treatment. Accordingly, using clinically applied RAD51 assay, we found that only pathogenic mutations in *BRCA2* were linked to homologous recombination deficiency in both CCA_PDX and advanced CCA patient samples. These preclinical insights suggest that patients with advanced CCA with pathogenic mutations of *BRCA2* may benefit from PARPi treatment, and those with pathogenic mutations of *IDH1*, *ARID1A*, or *BAP1* should be prioritized for other therapeutic options.

concordant with those found in patients with cancer (6, 7). Thus, they have become a valuable tool in oncology for evaluating new treatments and identifying biomarkers (8, 9). While a few collections of PDX models of CCA have been reported, most of them were derived from surgically resected primary tumors (10, 11). To date, PDX models focused on unresectable advanced CCA are not fully developed.

Pathogenic mutations in genes encoding for isocitrate dehydrogenase 1 (*IDH1*) and 2 (*IDH2*), AT-rich interaction domain 1A (*ARID1A*) and B (*ARID1B*), BRCA1-associated protein 1 (*BAP1*), and BRCA1/2 DNA repair associated (*BRCA1* and *BRCA2*) have been reported in 30%–50% of patients with CCA (12–16). Given their prevalence in CCA, among other types of malignancy, these mutations (*IDH1/2*[mut], *ARID1A/B*[mut], *BAP1*[mut], and *BRCA1/2*[mut]) are becoming promising targets for developing new therapeutic strategies (1). Indeed, preclinical models in different types of tumors harboring these mutations showed enhanced sensitivity to PARP inhibitors (PARPi) due to a deficiency in the homologous recombination (HR) repair pathway (17–21). Nonetheless, it is still unclear whether PARPi treatment represents an effective targeted therapy for advanced CCAs harboring these mutations.

Here, we present a unique collection of PDX models derived from biopsy samples of patients with unresectable metastatic CCA (CCA_PDX). These CCA_PDXs recapitulate the histopathologic and molecular features of their original tumor. In addition, when cultured *ex vivo*, tumor cells derived from CCA_PDX can form tumoroids that demonstrate concordant drug responses to those found in the original PDXs and patients with CCA. Notably, while we observed that PARPi inhibits tumor growth in *BRCA2*[mut] CCA tumoroids and PDXs, this effect was not found in the patient-derived models with *IDH1*[mut], *ARID1A*[mut], or *BAP1*[mut]. In agreement, using clinically applied RAD51 score assay (22–27), we found that both CCA_PDX and advanced CCA patient biopsy samples with *BRCA2*[mut], but not those with *IDH1/2*[mut], *ARID1A*[mut], or *BAP1*[mut], showed RAD51 scores compatible with an HR deficiency profile (HRD). These data suggest that patients with advanced CCA with *BRCA2*[mut] are likely to benefit from PARPi treatment in the clinic, and ongoing clinical trials should be prioritized.

Materials and Methods

Human specimens

CCA metastatic lesions (∼1–2 cm long, ∼1–2 mm diameter) were obtained by ultrasound-guided core needle biopsy, and one primary tumor sample was obtained during surgery. All procedures were performed in the Vall d'Hebron Hospital with informed written consent from patients. The studies were conducted in accordance with the Declaration of Helsinki. Human samples were handled and processed following the institutional guidelines under protocols approved by the Institutional Review Boards at the Vall d'Hebron Hospital prior to tissue acquisition. Each tumor biopsy specimen was divided into two parts: (i) formalin-fixed paraffin embedding (FFPE) and (ii) subcutaneous implantation into NOD.CB-17-Prkdc scid/Rj mice (Janvier Labs, RRID:MGI:3760616) for CCA_PDX generation. CCA diagnosis on biopsied samples was confirmed by histopathologic assessment.

Generation of CCA_PDXs

Tumor pieces (15–60 mm³) from patient metastatic lesions (except one from the primary tumor) were obtained from biopsy and immediately subcutaneously implanted into 6-week-old female NOD.CB-17-Prkdc scid/Rj mice (Janvier Labs, RRID:MGI:3760616). Animals were housed in air-filtered flow cabinets with a 12:12 light/dark cycle, and food and water were provided *ad libitum*. Upon growth of the engrafted tumors, a tumor piece was implanted into a new recipient mouse for the model perpetuation. Flash-frozen and FFPE samples were taken for genotyping and histologic studies in each passage. The presented collection of CCA_PDX is a part of the EuroPDX consortium (http://www.europdx.eu). All animal procedures were approved by the Ethical Committee for the Use of Experimental Animals at the Vall d'Hebron Institute of Research and by the Catalan Government.

IHC and image analysis

CCA_PDX and patient tumors were fixed immediately after excision in 4% buffered formalin solution for a maximum of 24 hours at room temperature before being dehydrated and paraffin embedded. The following primary mAbs were used for IHC staining: anti-KRT19 (Atlas Antibodies, catalog no. HPA002465, RRID: AB_1079179), anti-HepPar1 (Novus, catalog no. NBP3-08970, RRID:AB_2909615), anti-Ki67 (Roche, catalog no. 05278384001, RRID:AB_2631262), anti-cleaved caspase 3 (Asp175; Cell Signaling Technology, catalog no. 9661, RRID:AB_2341188) and secondary anti-rabbit (Jackson ImmunoResearch Labs, catalog no. 711-035-152, RRID:AB_10015282) and anti-mouse (Thermo Fisher Scientific, catalog no. G-21040, RRID:AB_2536527), and UltraMap anti-Rabbit antibody (horseradish peroxidase; Roche, catalog no. 05269717001, PRID:AB_2924783). For KRT19 and HepPar1 IHC, fixed tissue samples embedded in paraffin were sectioned to a 3-μm thickness. Sections were heated to 60°C, deparaffinized with xylene (131769.1612; Panreac), and hydrated with three steps of incubation with ethanol (from 100%, 96%, and 70%). For antigen retrieval, samples were boiled for 7 minutes in citrate buffer at pH 6 for KRT19 staining or at pH 9 for HepPar1 staining. Endogenous peroxidase was blocked by incubating the samples with 3% peroxide hydrogen (#108597, Merck Millipore) diluted in phosphate-buffered saline (PBS) for 10 minutes. Slides were permeabilized for 15 minutes in PBS with 1% Tween (A4974,0500, Panreac) and blocked with 3% bovine serum albumin (BSA) in 1× PBS for 1 hour; samples were then incubated overnight at 4°C, with the primary antibody

anti-KRT19 (Atlas Antibodies, catalog no. HPA002465, RRID: AB_1079179) diluted 1:200 or with HepPar1 (Novus, catalog no. NBP3-08970, RRID:AB_2909615) diluted 1:500, in blocking buffer and then incubated at room temperature for 1 hour with anti-rabbit or anti-mouse secondary antibody (Thermo Fisher Scientific, catalog no. G-21040, RRID:AB_2536527) at a 1:250 dilution. Samples were stained with DAB substrate chromogen (#K3468, Agilent) for 1–10 minutes and counterstained with Harris hematoxylin (#109254; Sigma) for 2 minutes, followed by dehydration with ethanol and xylene, and finally mounted in DPX (06522, Sigma). Positive and negative controls were run along the tested slides for each marker. For Ki67 and cleaved caspase 3 staining, slides were heated in the instrument at 75°C for 8 minutes and deparaffinized with EZ prep solution (Ventana Medical System, catalog no. 950-102 2L). Antigen retrieval was performed at 95°C for 64 minutes using the Cell Conditioning 1 buffer (CC1; Ventana Medical System, catalog no. 950-124 2L). Subsequent incubation of 8 minutes with CM inhibitor (ChromoMap DAP kit) was used for peroxidase blockade. For primary antibodies anti-Ki67 (prediluted; Roche, catalog no. 05278384001, RRID:AB_2631262) and anti-cleaved caspase 3 (Cell Signaling Technology, catalog no. 9661, RRID:AB_2341188; 1:100), slides were first incubated at 37°C for 24 or 60 minutes, respectively, and for further 8 minutes with UltraMap anti-Rabbit antibody (horseradish peroxidase; Roche, catalog no. 05269717001, PRID:AB_2924783). As a detection system, CM ChromoMap DAB kit (Roche Diagnostics, catalog no. 760-159) was used according to the manufacturer's instructions, followed by counterstaining with hematoxylin II (Ventana Medical System, catalog no. 760-2021) for 8–12 minutes and bluing reagent (Ventana Medical System, catalog no. 760-2037) for 4 minutes, dehydration, and mounting processes. Slides were scanned in the NanoZoomer 2.0-HT slide scanner (Hamamatsu Photonics) and visualized in the NDP.view2 software (Hamamatsu Photonics) or QuPath (28).

Genomic profiling

Molecular profiling was performed using FFPE tumor tissue obtained from patient biopsies and corresponding PDXs. For patient samples, DNA was analyzed using FoundationOne CDx hybrid-capture next-generation sequencing (NGS) service platform, an assay designed to detect substitutions, insertions, deletions, and rearrangements in a total of 324 genes, including genes known to be somatically altered in solid tumors that are validated targets for therapy (either approved or in clinical trials) and unambiguous drivers of oncogenesis based on current knowledge. For PDX samples, an in-house NGS panel was used for genomic characterization. Four 8-μm tissue sections from all PDXs, with more than 20% tumor area, were obtained, and DNA extraction was performed with the automated system Maxwell16 FFPE plus LEV DNA purification kit (Promega, catalog no. TM349). DNA quality and concentration were measured by Qubit and analyzed by NGS with a custom 435-gene hybrid capture-based panel (VHIO-300 panel, see Supplementary Table S1). Sequencing reads were aligned (BWA v0.7.17, Samtools v1.9) against a custom reference containing all chromosomes from hg19 mm10 reference genomes. Reads aligned to chromosomes from the mm10 genome were removed, and reads aligned to the hg19 genome were further analyzed. Picard (v1.139) was used to remove duplicates. Base recalibration, indel realignment (GATK v3.7.0), and variant calling (VarScan2 v2.4.3, Mutect2 v4.1.0.0) were performed. Variants from both callers are reported. A minimum of 7 reads supporting the variant allele were required to call a mutation. The technique's sensitivity is 5% MAF for single-nucleotide variants and 10% MAF for INDELs. Copy-number alterations were calculated with CNVkit (v0.9.6.dev0) using an in-house 2N pool as the standard sample. For somatic variant analysis, frequent SNPs in the population were filtered on the basis of the gnomAD database (allele frequency ≤ 0.0001). Variants were manually curated, and identified variants were classified using publicly available databases: COSMIC (RRID: SCR_002260), cBio-Portal (RRID: SCR_014555), ClinVar (RRID: SCR_006169), Var-Some, and OncoKB (RRID: SCR_014782).

CCA tumoroid *ex vivo* three-dimensional cultures

CCA patient-derived tumor cells were isolated from CCA_PDX through a combination of mechanic disruption and enzymatic disaggregation following a described protocol (4). Briefly, PDX tumors with a volume of less than 500 mm^3 were freshly collected in DMEM/F12/HEPES (L0093-500, Biowest) after surgical resection, minced using sterile scalpels, and dissociated for a maximum of 90 minutes in DMEM/F12/HEPES supplemented with 0.3 mg/mL collagenase (C9891, Sigma-Aldrich), 0.1 mg/mL hyaluronidase (H3506, Sigma-Aldrich), 2% BSA (VWRC0332, VWR), 5 μg/mL insulin (I1882, Sigma-Aldrich), and 50 μg/mL gentamycin (15750-037, Gibco). After centrifugation, pellets were further dissociated using 0.05% trypsin (HYCLSH30236.02, VWR), 5 mg/mL Dispase (7923, STEMCELL Technologies) and 1 mg/mL DNase (D4263, Sigma-Aldrich). Red blood cells were eliminated by washing the cell pellet with 1× Red Blood Cell Lysis Buffer solution (00-4333-57, eBioscience). Cells were then resuspended in DMEM/F12/HEPES supplemented with 2% of fetal bovine serum (10270106, Gibco), 1% penicillin/streptomycin (15140122, Gibco), 10 μg/mL of ROCK inhibitor (S1049, Selleck Chemicals) and 5 μg/mL insulin. For drug efficacy tests, cells were seeded at 4×10^4 cells/well on Matrigel precoated 48-well plates (130187, Thermo Fisher Scientific) or at 2×10^4 cells/well in a Matrigel pre-coated Corning 96-Well White Polystyrene Microplate (CLS3610, Corning). On the following day, cells were treated with either vehicle (DMSO) or the corresponding drug and cultured at 37°C in 5% of CO_2. Medium and treatments were refreshed every 2–3 days.

Cell viability measurement

Cell viability was evaluated at four different timepoints for growth kinetics on days 1, 4, 7, and 10. For each measurement, the culture medium was first replaced by cold PBS-ethylenediaminetetraacetic acid (EDTA) 1 mmol/L and incubated for 1 hour at 4°C to melt Matrigel; cell pellets were then obtained by centrifugation at 450 × g for 5 minutes at 4°C. The supernatant was removed, and pellets were resuspended with 50 μL of PBS with 1 mmol/L EDTA and transferred to a Corning 96-Well White Polystyrene Microplate. Cell viability was quantified using CellTiter-Glo Luminescent Cell Viability Assay (Promega; G7570), according to the manufacturer's instruction. Luminescence was measured with infinite M2000 Pro (Tecan) and i-control 1.11 software. For drug efficacy experiments, cells were treated *ex vivo* with the indicated compounds for 7 days, and cell viability was measured by CellTiter-Glo. As cells were already seeded in the final readout plate (Corning 96-Well White Polystyrene Microplate, CLS3610, Corning), Matrigel was melted by direct on-plate incubation with 50 μL PBS with1 mmol/L EDTA for 1 hour at 4°C. Cell viability was evaluated as described above.

Drug efficacy studies *in vivo*

Upon xenograft growth (50–150 mm³), CCA_PDX-bearing mice were randomized and treated with indicated molecules. NEO2734 was provided by Epigene Therapeutics Inc. and dissolved in PEG300 (81162-1L, Sigma-Aldrich). Olaparib (AZD2281) was
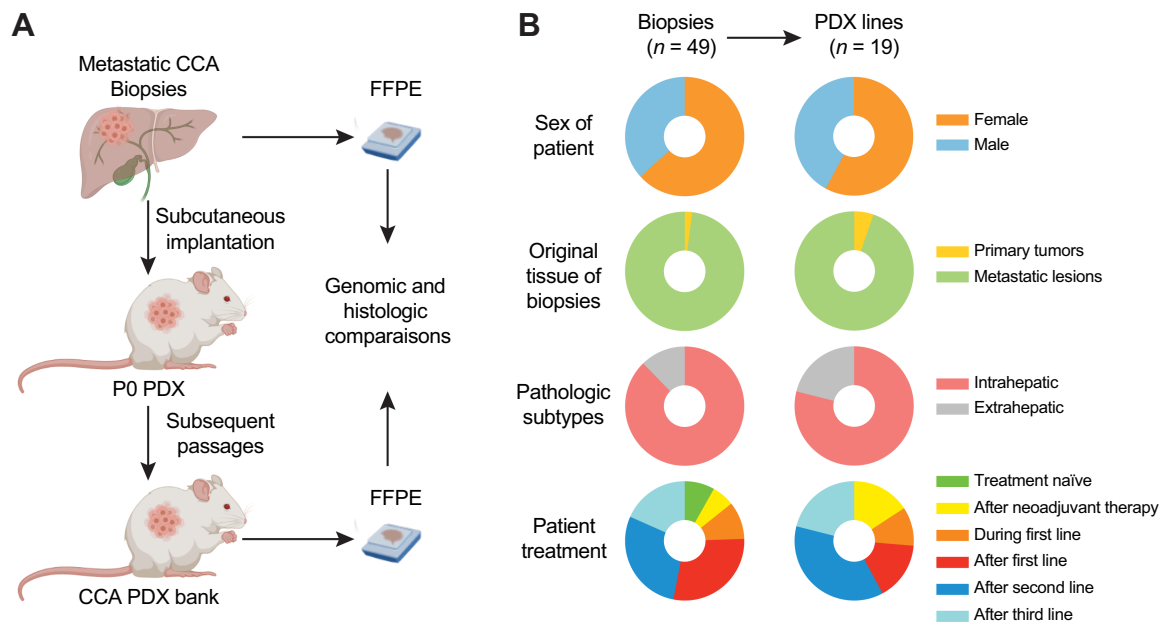
Figure 1.
Generation of CCA_PDX models. **A,** Schematic illustration of the process of establishing and maintaining CCA_PDXs. Successfully established CCA_PDXs are compared with their foundation biopsy counterparts in histologic and genomic analyses. **B,** Pie charts showing the stratification of all biopsies ($n = 49$) and successfully established CCA_PDXs ($n = 19$) based on the sex of the patient, tissue origin of biopsies, pathologic subtypes, and patient treatment received prior to biopsy.

purchased from MedChemExpress (catalog no. HY-10162) and dissolved in 10% DMSO (v/v) and 10% Kleptose [HP-β-CD] (346102, Roquette) (w/v). Pamiparib was provided by BeiGene and dissolved in sterilized 0.5% methylcellulose (M0262, Sigma-Aldrich). Niraparib (MK-4827; catalog no. HY-10619) and pemigatinib (INCB054828; catalog no. HY-109099) were purchased from Med-ChemExpress. Each treatment regimen is indicated in the figures. Tumor growth was measured 3× per week with a caliper; researchers were blinded to the treatment effect. Mice weights were recorded 3× per week. Tumor volumes were calculated using the formula:

Table 1. Characteristics of patients with metastatic CCA, biopsies, and PDXs.

		Biopsies Total ($n = 49$) n (%)	Unsuccessful engraftment ($n = 30$) n (%)	Successful engraftment ($n = 19$) n (%)	P
Sex of patient					0.7516
	• Female	31 (63.3)	20 (66.7)	11 (57.9)	
	• Male	18 (36.7)	10 (33.3)	8 (42.1)	
Median patient age at biopsy (years) [interquartile range]		59 [49–70.5]	61 [40–70.8]	57 [48–71]	0.262
Original tissue of biopsies					0.8160
	• Primary tumors	1 (2.0)	0 (0)	1 (5.3)	
	• Metastatic lesions	48 (98.0)	30 (100)	18 (94.7)	
CCA pathologic subtypes					0.2939
	• Intrahepatic	43 (87.8)	28 (93.3)	15 (78.9)	
	• Extrahepatic	6 (12.2)	2 (6.7)	4 (21.1)	
Patient treatment					0.0777
	• Treatment naïve	4 (8.2)	4 (13.3)	0 (0)	
	• After adjuvant treatment (gemcitabine + capecitabine)	3 (6.1)	0 (0)	3 (15.8)	
	• During first line (gemcitabine + platinum)	5 (10.2)	3 (10.0)	2 (10.5)	
	• After first line (gemcitabine + platinum)	14 (28.6)	11 (36.7)	3 (15.8)	
	• After second line (chemotherapy or targeted therapy)	14 (28.6)	7 (23.3)	7 (36.8)	
	• After third line	9 (18.4)	5 (16.7)	4 (21.1)	
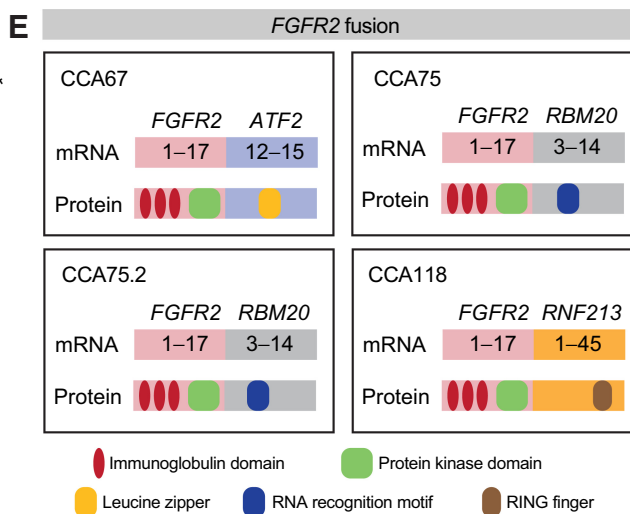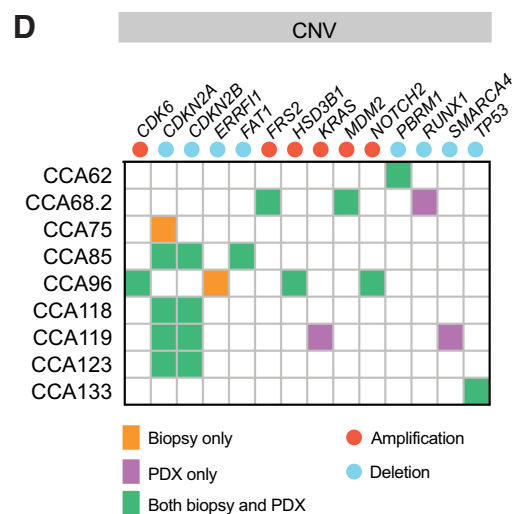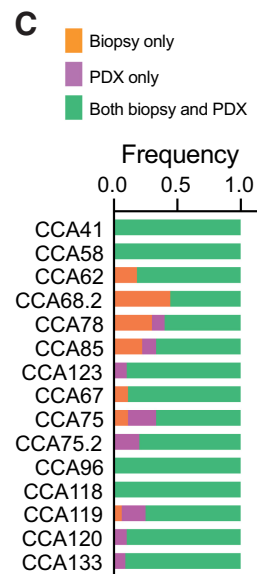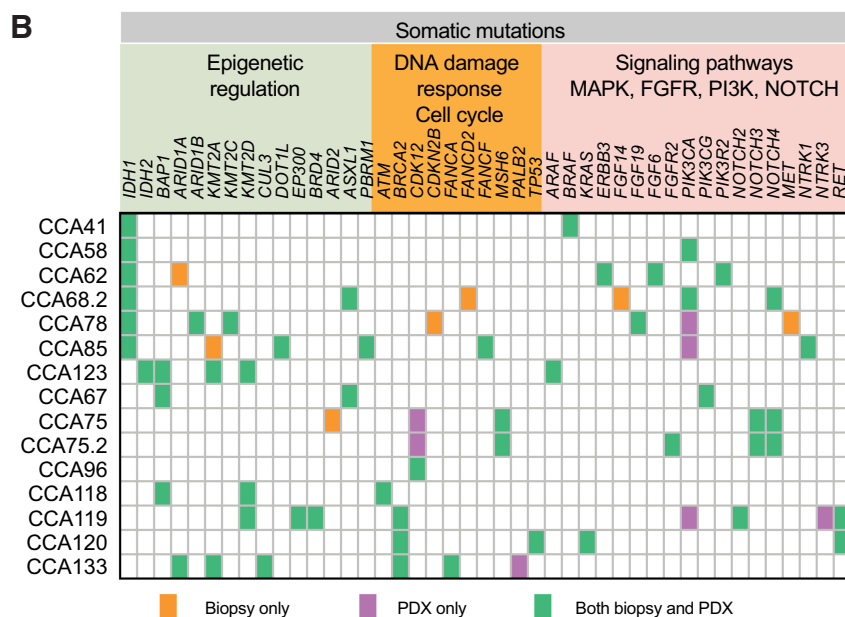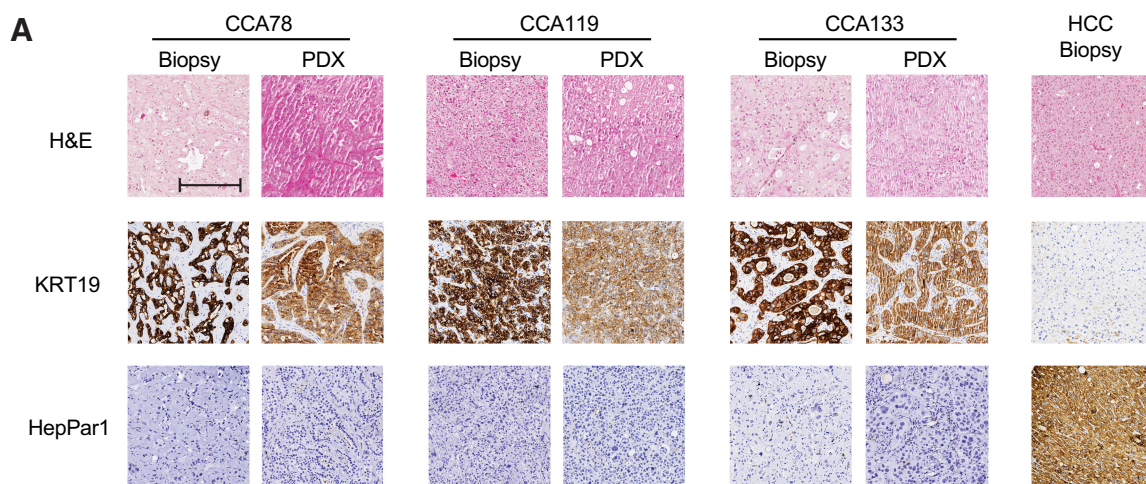
$V = (\text{length} \times \text{width}^2)/2$. According to institutional guidelines, mice were euthanized using CO_2 inhalation once tumors reached 1–1.5 cm^3 or in case of severe weight loss.

Immunofluorescence staining

For immunofluorescence staining, cells were seeded on a Matrigel precoated 8-well Nunc Lab-Tek Chamber Slide system (C7182, Thermo Fisher Scientific) at 4×10^4 cells/well. After a 72-hour to 144-hour incubation, cells were fixed with 4% paraformaldehyde (30525-89-4, Santa Cruz Biotechnology) for 15 minutes, washed with 1% BSA in PBS for 5 minutes, and permeabilized with 1% Triton X-100 for 20 minutes at room temperature. After 1 hour of blocking in 5% BSA-PBS, cells were incubated at room temperature for 2 hours with the primary antibody anti-KRT19 (Atlas Antibodies, catalog no. HPA002465, RRID:AB_1079179) or anti-HepPar1 (Novus, catalog no. NBP3-08970, RRID:AB_2909615) diluted 1:200 in blocking buffer. Cells were then incubated for 1 hour with a secondary anti-rabbit antibody (Jackson ImmunoResearch Labs, catalog no. 711-035-152, RRID:AB_10015282) diluted at 1:400 in blocking buffer, washed twice with 1% BSA PBS, and incubated with 4′,6-diamidino-2-phenylindole (DAPI; D9542, Sigma-Aldrich) in PBS for 5 minutes. Slides were then mounted with Fluoromount-G (0100-01, SouthernBiotech). Slides were stored at 4°C until analysis. Images were acquired with a Nikon confocal microscope C2+ equipped with an LU-N4S laser unit, using the NIS-Elements software (Nikon).

RAD51 assay

A total of 3-μm FFPE sections from patients with CCA and PDXs were used for the analysis of RAD51 foci (as a functional readout of HRD) and γH2AX foci (as a biomarker of endogenous double-stranded DNA damage); each biomarker was counterstained with geminin (as a marker of the S–G$_2$ cell-cycle phase) and DAPI, as described previously (26, 27). The following primary antibodies were used for immunofluorescence: rabbit anti-RAD51 (Abcam, catalog no. ab133534, RRID:AB_2722613, 1:1,000), mouse anti-γH2AX (Millipore, catalog no. 05-636, RRID:AB_309864, 1:200), mouse anti-geminin (Leica Biosystems, catalog no. NCL-L-Geminin, RRID:AB_563738, 1:60), and rabbit anti-geminin (Proteintech, catalog no. 10802-1-AP, RRID:AB_2110945, 1:400). Goat anti-rabbit Alexa fluor 568 (Thermo Fisher Scientific, catalog no. A-11036, RRID:AB_10563566), goat anti-mouse Alexa Fluor 488 (Thermo Fisher Scientific, catalog no. A-28175, RRID:AB_2536161), donkey anti-mouse Alexa Fluor 568 (Thermo Fisher Scientific, catalog no. A-10037, RRID:AB_2534013), and goat anti-rabbit Alexa Fluor 488 (Thermo Fisher Scientific, catalog no. A-11070, RRID:AB_2534114; 1:500) were used as secondary antibodies. Scoring was carried out blindly using live images and a 60× immersion oil lens in a Nikon Ti-Eclipse microscope. The mean score from two observers is provided for each sample. At least 40 geminin-positive cells were analyzed per sample, and the γH2AX score was used as a quality check to ensure the presence of enough endogenous DNA damage to evaluate homologous recombination repair functionality (cutoff, 25% geminin-positive cells with γH2AX foci). The RAD51 score was considered low or high based on the predefined cutoff of 10% geminin-positive cells with ≥5 RAD51 nuclear foci.

Statistical analysis

χ^2 tests were used to search for associations between PDX engraftment and categorical clinical features of the patients; Mann–Whitney U tests were used for detecting various clinical features. These tests were performed using Python 3.6.12 (RRID:SCR_001658) and the Scipy 1.5.2 package. Unless otherwise stated, statistical tests were performed with GraphPad Prism Version 9.4.1 (RRID:SCR_002798) with methods indicated in the figure legends.

Data availability

Next-generation panel sequencing data have been deposited in the NCBI BioProject (https://www.ncbi.nlm.nih.gov/bioproject) under BioProject number PRJNA763182. The data generated in this study are available within the article and its Supplementary Data. The data supporting the findings of this study are also available from the corresponding author upon reasonable request.

Results

PDX models were generated from biopsies of patients with unresectable metastatic CCA

We generated PDX models from biopsy specimens collected over 5 years (from 2016 to 2020) from 49 patients with a confirmed diagnosis of metastatic CCA (**Fig. 1A**; Supplementary Table S2). Of note, specimens from 48 patients with the unresectable disease (98%) were obtained by ultrasound-guided biopsy of metastatic lesions, and one specimen (2%) was obtained by biopsy of the primary tumor during surgery (**Fig. 1B**; **Table 1**). Forty-three patients (87.8%) were diagnosed with intrahepatic CCA and 6 (12.2%) with confirmed extrahepatic CCA. Importantly, 45 of the 49 patients (91.8%) had already received at least one line of platinum-based chemotherapy, neoadjuvant chemotherapy, and/or targeted therapy; only 4 (8.2%) were treatment naïve.

Patient specimens were subcutaneously implanted into immune-deficient (NOD/SCID) mice immediately after the biopsy procedure to generate CCA_PDX models. The establishment of CCA_PDX models was determined to be successful based on whether they: (i) could be readily and serially transplanted; (ii) recapitulated the histopathologic characteristics of the initial biopsy sample; (iii) reliably retained the main genomic alteration of the initial biopsy tissue. Of the 49 implanted samples, 19 generated CCA_PDX models (success rate, 38.8%), with a median latency (e.g., time from implantation in mice to

Figure 2.
CCA_PDXs maintain the histologic and genomic features of the original biopsy specimens. **A,** Comparative histologic and IHC images of tumors of CCA_PDXs compared with each original biopsy specimen. Top row, H&E staining; middle row, IHC staining of KRT19 (CCA marker); and bottom row, IHC staining of HepPar1 (HCC). Representative examples of 19 CCA_PDXs are shown; an HCC biopsy sample was used as a control. CCA_PDX samples were collected at passage 1 (PDX133) or passage 2 (PDX78 and PDX119). Scale bar, 250 μm. **B,** Comparison of somatic mutations identified in CCA_PDX tumors and their parental biopsy specimens. Genes harboring mutations were classified into three categories: epigenetic regulation, DNA damage response/cell-cycle control, and signaling pathways. CCA_PDX samples were collected at passage 1 (PDX41, PDX123, PDX96, PDX118, and PDX133) or passage 2 (PDX58, PDX62, PDX68.2, PDX78, PDX85, PDX67, PDX75, PDX75.2, PDX119, and PDX120). **C,** Frequencies of mutations identified as biopsy-specific, PDX-specific, or common somatic mutations. **D,** Comparison of CNVs identified in CCA_PDX tumors and the original biopsy samples. **E,** Diagrams of *FGFR2* gene fusions identified in four paired biopsy–PDX samples. Fusion mRNAs (including *FGFR2*) and their fusion partners are indicated, as well as the predicted protein products of the fusions with their functional domains. Numbers represent the exon of the corresponding genes.

tumor growth) of 4.7 months (Supplementary Fig. S1A). Importantly, these 19 CCA_PDXs proportionally represented the original 49 patients in regard to patient sex, original tissue, pathologic subtypes, and treatment received (**Fig. 1B**), suggesting that none of these factors was associated with the success and/or failure of PDX generation; this was confirmed by further statistical analyses (**Table 1**). Thus, we successfully generated a panel of 19 PDXs using biopsy specimens from patients with unresectable metastatic CCA who had been previously treated.

The CCA_PDX characteristics match those of the original biopsy tissues

We next investigated whether the histopathologic characteristics of the original biopsy samples were preserved in the CCA_PDXs. Histopathologic analyses of hematoxylin and eosin (H&E)-stained tissue showed features in the PDXs consistent with CCA and with similarities to the original biopsy specimens (**Fig. 2A**). Moreover, as the majority of our CCA_PDX collection was generated using biopsy samples from liver metastatic lesions (17 of 19 PDX), we also used cytokeratin 19 protein (KRT19) and hepatocyte paraffin 1 (HepPar1) as biomarkers to distinguish CCA (which is KRT19+/HepPar1−) from HCC (which is KRT19−/HepPar1+; ref. 29). IHC analysis revealed that all CCA_PDXs and their original biopsy specimens were KRT19+/HepPar1−, further confirming the CCA identity (**Fig. 2A**; Supplementary Fig. S2A). As expected, the HCC biopsy sample used as a control was KRT19−/HepPar1+.

To verify whether the CCA_PDXs faithfully recapitulated the genomic features of each corresponding original biopsy specimen, the genomic DNA samples from fifteen original biopsy samples and their corresponding CCA_PDXs were sequenced (by Foundation Medicine for the biopsies, and in-house NGS with a custom 435-gene hybrid capture-based panel for the CCA_PDXs). Notably, we found that the CCA_PDX models maintained most of the somatic mutations identified in the corresponding original biopsy specimens (**Fig. 2B and C**; Supplementary Tables S3 and S4). Many of these identified somatic mutations were in genes involved in epigenetic regulation (e.g., *IDH1, IDH2, BAP1, ARID1A/B*), DNA damage and cell-cycle control (e.g., *BRCA2, TP53*), or signaling pathways (e.g., *BRAF, PIK3CA*), corresponding to previous reports (12, 13, 16, 30). Analysis of copy-number variation (CNV) revealed a high similarity between CCA_PDXs and the paired original biopsy samples (**Fig. 2D**). We also detected amplification of putative oncogene *MDM2* and homozygous deletions of *CDKN2A*, which have been associated with the CCA pathology (13). Finally, we analyzed the *FGFR2* fusion status, as *FGFR2* fusion genes have been observed in 10%–15% of CCA patient samples (15, 16). We found three types of predicted *FGFR2* fusions in four original biopsy samples as well as in the corresponding CCA_PDXs (**Fig. 2E**; Supplementary Fig. S3A). The identified fusions involve the 5′-part of the *FGFR2* gene, which encodes for an intact tyrosine domain, fused in-frame with 3′-part of the gene encoding the transcription factor activating transcription factor 2 (ATF2; CCA67), the RNA-binding protein RNA-binding motif protein 20 (RBMC20; CCA75 and CCA75.2), and the ring finger protein 123 (RNF213; CCA118). Therefore, in both the histopathologic and genomic analyses, the CCA_PDXs faithfully recapitulated the key features of their original biopsy specimens.

Short-term *ex vivo* three-dimensional culture of CCA_PDX-derived cells for evaluating drug efficacy

Although PDX models are valuable for preclinical studies, expanding these models *in vivo* for drug efficacy evaluation is

costly and time consuming. Several studies have demonstrated that tumor cells derived from PDXs can be maintained in *ex vivo* three-dimensional (3D) culture systems and used for "pre–*in vivo*" drug screens (4, 31–33). Importantly, the drug responses obtained from these *ex vivo* culture systems are highly predictive of those from their *in vivo* PDX counterparts. We therefore aimed to establish and optimize a short-term *ex vivo* 3D culture protocol for tumor cells derived from our CCA_PDXs (**Fig. 3A**). Briefly, single-cell suspensions were obtained from CCA_PDXs and seeded out on a Matrigel pre-coated dish; after 24 hours, tumoroids began to form at the interface between the culture medium and Matrigel (see Materials and Methods). These tumoroids could be grown in culture for at least 10 days (**Fig. 3B**; Supplementary Fig. S4A), and they maintained CCA histopathologic features and marker expression (e.g., KRT19+/HepPar1−; **Fig. 3C**).

To test whether this system can be used as a platform for preclinical drug efficacy evaluation, we first focused on a novel bromodomain and extraterminal domain (BET) inhibitor, NEO2734. BET inhibitors have demonstrated efficient antitumor activities in both hematopoietic and solid tumors, including CCA (34–38). NEO2734 is a novel potent BET-CBP/p300 dual inhibitor, and its antitumoral activity has been shown using *in vitro* cell lines, *ex vivo* organoids, and *in vivo* PDX of multiple cancer types (39–42). We found that NEO2734 showed significant antiproliferative effects in tumoroids derived from different CCA_PDXs, with an average IC_{50} of 685.3 nmol/L (**Fig. 3D**), indicating its potential application for CCA treatment. Next, we verified whether the results obtained in CCA tumoroids were predictive of the drug response observed in CCA_PDXs *in vivo*. For this, CCA_PDX78 was first expanded in NOD-SCID mice and then treated with vehicle or NEO2734. In agreement with the results obtained in the *ex vivo* 3D culture system, NEO2734 significantly inhibited the CCA_PDX78 tumor growth *in vivo* (**Fig. 3E**).

Furthermore, we also tested whether the CCA tumoroids can capture drug responses observed in patients with CCA. We used two CCA_PDX models derived from a patient with *FGFR2* fusion. The PDX75 was developed before FGFR inhibitor treatment and the PDX75.2 after therapy with progressive disease (**Fig. 3F**). We found that tumoroids derived from PDX75 were more sensitive to FGFR inhibitor pemigatinib treatment than those derived from PDX75.2 (**Fig. 3G**). Of note, in PDX75.2 and the corresponding patient biopsy samples, we could identify *FGFR2* V564 L mutation, which has been associated with acquired resistance to FGFR inhibitor in CCA (Supplementary Table S4; refs. 43–45).

Thus, we have established a short-term, *ex vivo* 3D culture system for tumor cells derived from CCA_PDXs; this CCA tumoroid culture system can be used for rapid drug efficacy tests. Notably, the results obtained from this system agreed with those observed in CCA_PDXs and patients with CCA.

PARPi treatment inhibits the growth of *BRCA2*[mut] CCA_PDX

Pathogenic mutations of *IDH1/2, ARID1A/B, BAP1*, and *BRCA1/2* have been found in many types of solid tumors (46), including 30%–50% of patients with CCA (12–16). Efforts have thus been made to discover the vulnerability of cancer cells harboring these mutations and to design accordingly novel therapeutic strategies. Notably, the oncometabolite 2-hydroxyglutarate produced by mutant IDH1/2 enzymes, and loss of function of ARID1A, BAP1, or BRCA2 can impair the HR pathway, rendering cancer cells sensitive to PARPi treatment (18–21, 47, 48). However, preclinical evidence supporting the employment of PARP inhibition in advanced CCA with these mutations is still missing. Among our 19 established CCA_PDX
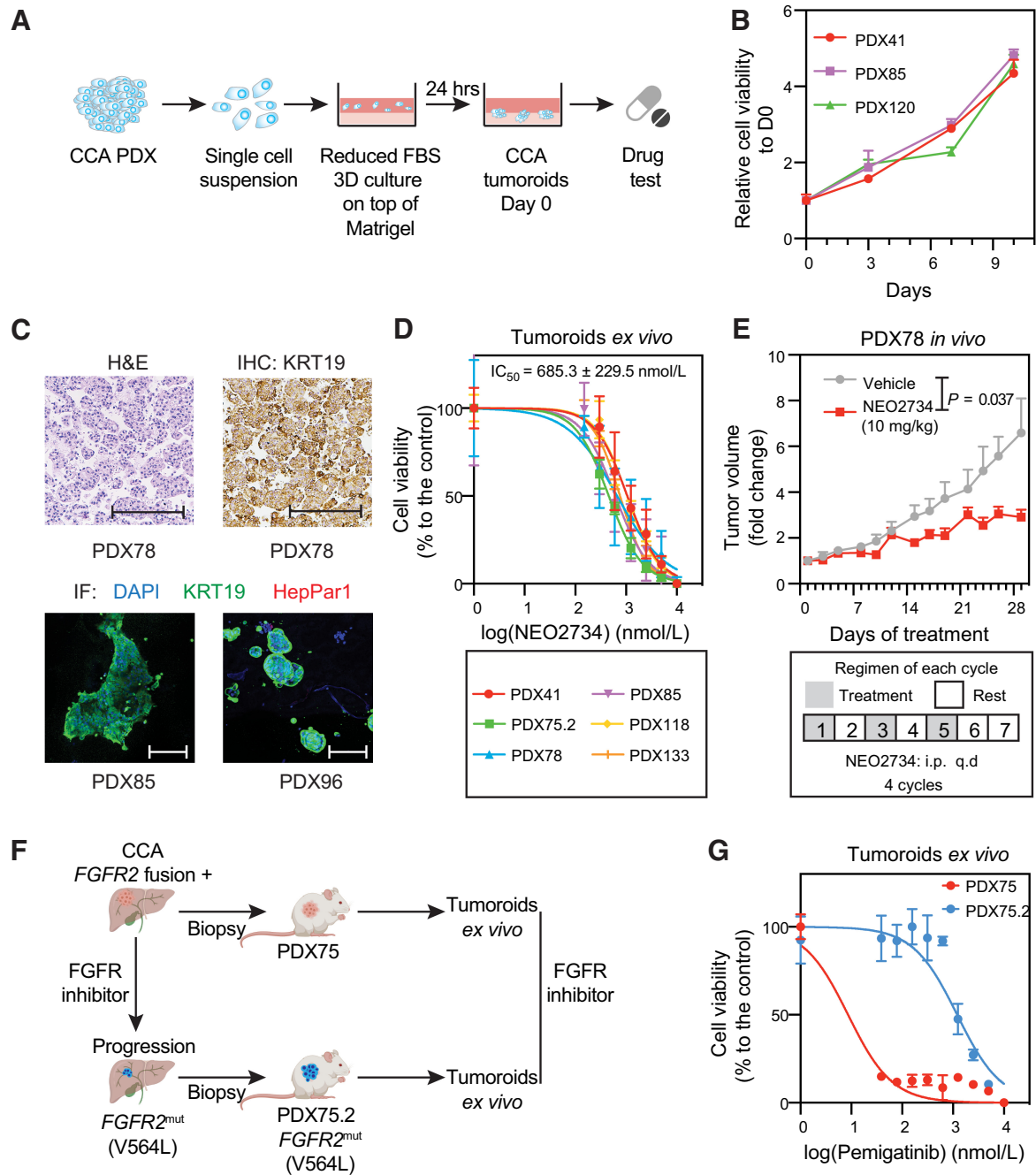
Figure 3.
Ex vivo 3D culture of tumors derived from CCA_PDXs can be used to evaluate drug efficacy. **A,** Schematic illustration of the process of *ex vivo* 3D culture of tumoroids derived from CCA_PDX. **B,** Cell proliferation of CCA_PDX-derived tumoroids was determined using CellTiter-Glo assays. Data were normalized to cell viability measured on day 0 (D0) and are mean $\pm$ SD from three independent replicates. **C,** Histopathologic characterization of tumoroids generated using CCA_PDX-derived cells cultured *ex vivo* for 10 days. Top row: H&E staining (left); IHC for the CCA marker KRT19 (right); bottom row: CCA marker KRT19 (left) and the HCC marker HepPAR1 (right); representative images are shown. Scale bars, 250 μm (top row), 50 μm (bottom row). **D,** NEO2734 dose–response curves for a panel of CCA_PDX-derived tumoroids cultured *ex vivo*. Cell viability was determined using Cell Titer-Glo assay on day 7. (The initiation of treatment was considered as day 1.) Data are mean $\pm$ SD from independent biological replicates (PDX41, $n = 5$; PDX75.2, $n = 2$; PDX78, $n = 6$; PDX85, $n = 6$; PDX118, $n = 3$; PDX113, $n = 3$). **E,** Effects of NEO2734 evaluated *in vivo* using CCA_PDX78. Mice implanted with PDX78 were treated intraperitoneally three times per week for 4 weeks with either vehicle ($n = 6$) or NEO2734 (10 mg kg^{-1}) ($n = 6$). Each tumor volume was normalized to its volume measured on day 1 of treatment. Data are mean $\pm$ SEM (multiple *t* tests); the *P* value was from data of day 29. **F,** Schematic illustration of the process of establishing two PDX models from a patient with CCA with *FGFR2* fusion (prior to FGFR inhibitor treatment and in progression) and using tumoroids derived from the paired PDXs to test the efficacy of FGFR inhibitor. **G,** FGFR inhibitor pemigatinib dose–response curves for PDX75- and PDX75.2-derived tumoroids cultured *ex vivo*. Cell viability was determined using Cell Titer-Glo assay on day 7. (The initiation of treatment was considered as day 1.) Data are mean $\pm$ SD from independent biological replicates (PDX75, $n = 3$; PDX75.2, $n = 3$).
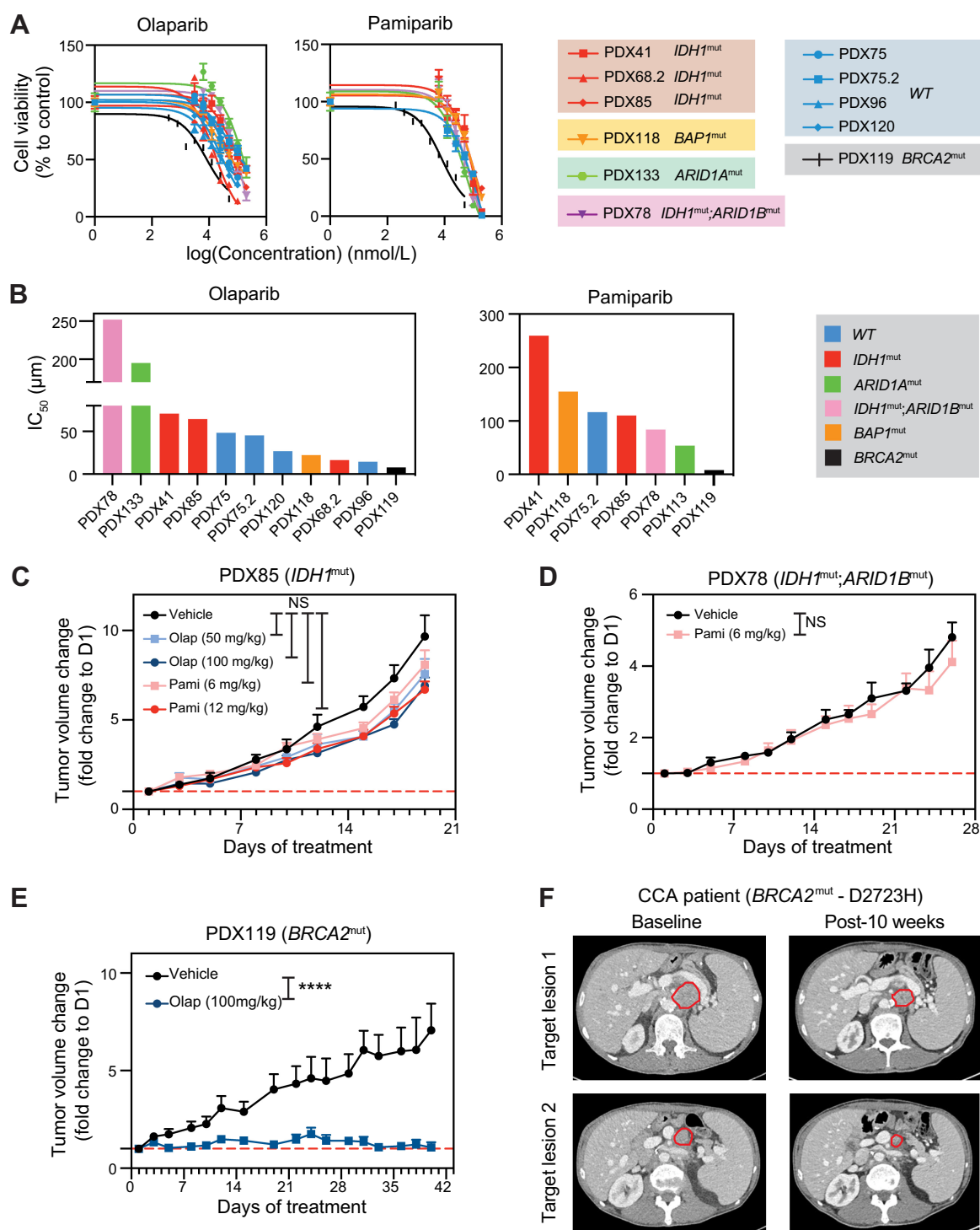
Figure 4.
PARPi inhibits the growth of CCA_PDXs with a *BRCA2* mutation. **A,** Dose–response curves of olaparib (left) or pamiparib (right) for a panel of tumoroids derived from CCA_PDXs. Cell viability was determined using a Cell Titer-Glo assay 7 days after the treatment initiation. Data are mean ± SD from independent biological replicates. For olaparib treatment: PDX41, $n = 8$; PDX68.2, $n = 2$; PDX78, $n = 6$; PDX85, $n = 11$; PDX75, $n = 2$; PDX75.2, $n = 4$; PDX96, $n = 2$; PDX118, $n = 3$; PDX120, $n = 2$; PDX133, $n = 3$; and PDX119, $n = 3$. For pamiparib treatment: PDX41, $n = 6$; PDX78, $n = 6$; PDX85, $n = 9$; PDX75.2, $n = 2$; PDX118, $n = 3$; PDX133, $n = 3$; PDX119, $n = 3$. **B,** IC$_{50}$ of olaparib (left) and pamiparib (right) in tumoroids derived from CCA_PDXs. **C,** Effects of olaparib and pamiparib evaluated *in vivo* using PDX85 (*IDH1*^{mut}). Mice implanted with PDX85 were treated orally six times per week with either vehicle ($n = 8$) or olaparib (at a low or high dose, of 50 or 100 mg kg^{-1}, respectively; each $n = 10$) or pamiparib (at a low or high dose, of 6 or 12 mg kg^{-1}, respectively; each $n = 8$). Each tumor volume was normalized to its volume on day 1 (D1). Data are mean ± SEM (two-way ANOVA multiple comparisons with Tukey correction); the indicated P value reflects data from D19.(*Continued on the following page.*)

models, 10 have confirmed pathogenic mutations of *IDH1* (*n* = 7), *ARID1A* (*n* = 1), *BAP1* (*n* = 1), or *BRCA2* (*n* = 1), and one with *ARID1A* deletion (Supplementary Table S4). We therefore checked the PARPi response in these CCA_PDXs.

We first tested the effects of each of three PARPis (i.e., olaparib, pamiparib, and niraparib) using established *ex vivo* 3D culture systems of tumor cells derived from CCA_PDXs harboring mutations in *IDH1*, *ARID1A*, *BAP1* or *BRCA2*. Of note, these PARPis are either approved by the FDA or are currently being evaluated in multiple clinical trials (17). As controls, we also included cells derived from CCA_PDXs harboring none of these mutations (wild-type CCA_PDXs). We found that, among all tumoroid models tested, only those derived from *BRCA2*[mut] CCA_PDX (PDX119) were sensitive to olaparib and pamiparib treatments (**Fig. 4A** and **B**). In contrast, neither tumoroids derived from wild-type CCA_PDXs nor those derived from CCA_PDXs harboring *IDH1*[mut], *ARID1A*[mut], or *BAP1*-[mut] were found sensitive to any of the three PARPi treatments (IC$_{50}$ >10 μmol/L; **Fig. 4A** and **B**; Supplementary Fig. S5A and S5B). Moreover, in line with these findings, although olaparib and pamiparib treatments did not affect the *in vivo* growth of PDX85 (*IDH1*[mut], R132C; **Fig. 4C**) or PDX78 (*IDH1*[mut], R132L; **Fig. 4D**), olaparib treatment significantly inhibited the tumor growth of PDX119 (*BRCA2*[mut], G3076R; **Fig. 4E**). Further IHC analysis for the cell proliferation marker Ki67 and the apoptosis marker cleaved caspase 3 revealed that PARPi treatment did not alter *IDH1*[mut] tumor cell proliferation or apoptosis in vivo (Supplementary Fig. S5C and S5D).

Moreover, a 73-year-old male patient with metastatic CCA with a pathogenic *BRCA2*[mut] (D2723H) was identified by NGS (Foundation-nOne Panel). This patient was initially diagnosed with localized extrahepatic CCA (T2N2M0), and had received surgical resection (R0) and adjuvant chemotherapy with capecitabine. Unfortunately, multiple metastatic lesions were found after the adjuvant chemotherapy, mainly localized in the celio-mesenteric lymph nodes. He then received cisplatin/gemcitabine, carboplatin/gemcitabine, and durvalumab/tremelimumab (as part of the IMMUNO-BIL clinical trial, NCT03704480) treatments. Because pathogenic *BRCA2*[mut] (D2723D) was identified in the tumor samples, he was compassionately treated with olaparib at a dose of 300 mg orally, twice a day continuously. After 10 weeks of treatment, CT scans showed regressions of several target lesions (**Fig. 4F**).

Thus, our results showed that PARPi treatments are effective in advanced CCA patient-derived preclinical models with *BRCA2*[mut], but not those harboring *IDH1*[mut], *ARID1A*[mut], or *BAP1*[mut]. In agreement, olaparib showed clinical activity in a patient with CCA with pathogenic *BRCA2*[mut].

RAD51 scoring predicts that patients with *IDH1*[mut], *ARID1A*[mut], or *BAP1*[mut] CCA may not benefit from PARPi treatment

The rationale for using PARPis to treat *IDH1/2*[mut], *ARID1A*[mut], *BAP1*[mut], or *BRCA2*[mut] tumors is based on the reported findings that cells harboring these mutations are defective for HR (18–21, 47, 48). As we only observed the expected antitumoral effects of PARPis in *BRCA2*[mut] CCA_PDX, and this effect was not found in tumoroids

and CCA_PDXs with *IDH*[mut], *ARID1A*[mut], or *BAP1*[mut], we next sought to examine the HR status of these CCA_PDXs to determine whether they are HR proficient (HRP) or HR deficient (HRD). We used a recently developed RAD51 assay to estimate HR status in routine FFPE tumor samples (26, 27). This assay analyzes nuclear immunofluorescence staining of the DNA repair protein RAD51 (RAD51), geminin, and DAPI. Tumors were considered HRP if more than 10% of geminin+ tumor cells had more than five RAD51+ foci (**Fig. 5A**). Otherwise, the tumor was scored as HRD. Moreover, immunofluorescence of the phosphorylation of the Ser-139 residue of the histone variant H2AX (γH2AX) was also scored on a consecutive slide to evaluate the basal DNA damage level of the tumor. Of note, the RAD51 assay has been applied in multiple clinical trials and PDX models, and tumors with HRD profiles scored by this assay showed responses to PARPis with high sensitivity and specificity (22–25).

Using this assay, we found that 17 of 18 tested CCA_PDXs showed RAD51 scores above 10% (**Fig. 5B**), which is compatible with an HRP profile. Only PDX119 and its original patient samples with a biallelic pathogenic *BRCA2* mutation showed, as expected, a RAD51 score below 10%, compatible with an HRD profile (**Fig. 5B**; Supplementary Fig. S6A). All samples showed significant DNA damage (γH2AX score median, 59%; interquartile range, 52%–74%). Importantly, *IDH1/2*[mut], *ARID1A/B*[mut], or *BAP1*[mut] CCA_PDXs were scored as HRP as wild-type CCA_PDXs (**Fig. 5B**). Moreover, we also confirmed that the original CCA biopsy specimens scored concordantly with their matched CCA_PDXs (Supplementary Fig. S6A), suggesting that the HR repair status observed was not due to the PDX setting but rather was representative of the patient sample of origin. These results demonstrated that, in this panel of CCA_PDXs, mutations of *IDH1/2*, *ARID1A/B*, or *BAP1* were not associated with an HRD profile, which would explain the absence of a PARPi treatment sensitivity in these CCA_PDXs. In line with these findings, we also found that the RAD51 scores increased in the PDX85 (*IDH1*[mut]) tumors treated with olaparib or pamiparib in vivo (Supplementary Fig. S6B), indicating that the HR repair pathway is still functional in these tumors.

To further strengthen our findings, we also analyzed an independent cohort of patients with metastatic CCA using the RAD51 assay (**Fig. 5C**; Supplementary Table S5). This analysis confirmed the HRD profiles in patients with CCA with pathogenic mutations of *BRCA2* (*n* = 2; **Fig. 5D**). In contrast, patients with CCA with pathogenic mutations of *IDH1/2*[mut] (*n* = 10), *ARID1A*[mut] (*n* = 3), or *BAP1*[mut] (*n* = 7) showed HRP profiles (**Fig. 5D**). We concluded that pathogenic mutations of *BRCA2*, but not those of *IDH1/2*[mut], *ARID1A*[mut], and *BAP1*[mut], are associated with HR deficiency profile, at least in metastatic CCA that has progressed following chemotherapy. Importantly, these data also suggest that patients with metastatic CCA with *BRCA2*[mut], but not those with *IDH1/2*[mut], *ARID1A*[mut], or *BAP1*[mut], are likely to benefit from PARPi treatment.

Discussion

PDXs have become an essential tool for understanding the mechanisms underlying cancer development and progression, and

(*Continued.*) **D,** Effects of pamiparib evaluated *in vivo* using PDX78 (*IDH1*[mut]). Mice implanted with PDX78 were treated orally with either vehicle (*n* = 5) or pamiparib (6 mg kg^{-1}; *n* = 5) six times per week. Each tumor volume was normalized to its volume measured on day 1 of treatment (D1). Data are mean ± SEM (multiple *t* tests); the indicated *P* value was from day 26. **E,** Effects of olaparib evaluated *in vivo* using PDX119 (*BRCA2*[mut]). Mice implanted with PDX119 were treated orally with either vehicle (*n* = 5) or olaparib (100 mg kg^{-1}; *n* = 5) six times per week. Each tumor volume was normalized to its volume measured on day 1 of treatment (D1). Data are mean ± SEM (multiple *t* tests); the indicated *P* value was from day 40. **F,** CT scan images of a 73-year-old male patient with metastatic CCA with a pathogenic *BRCA2* mutation at baseline and after 10 weeks of olaparib treatment. Target lesion 1 (adjacent to the splenic vein) and target lesion 2 (mesenteric) are outlined in red lines.
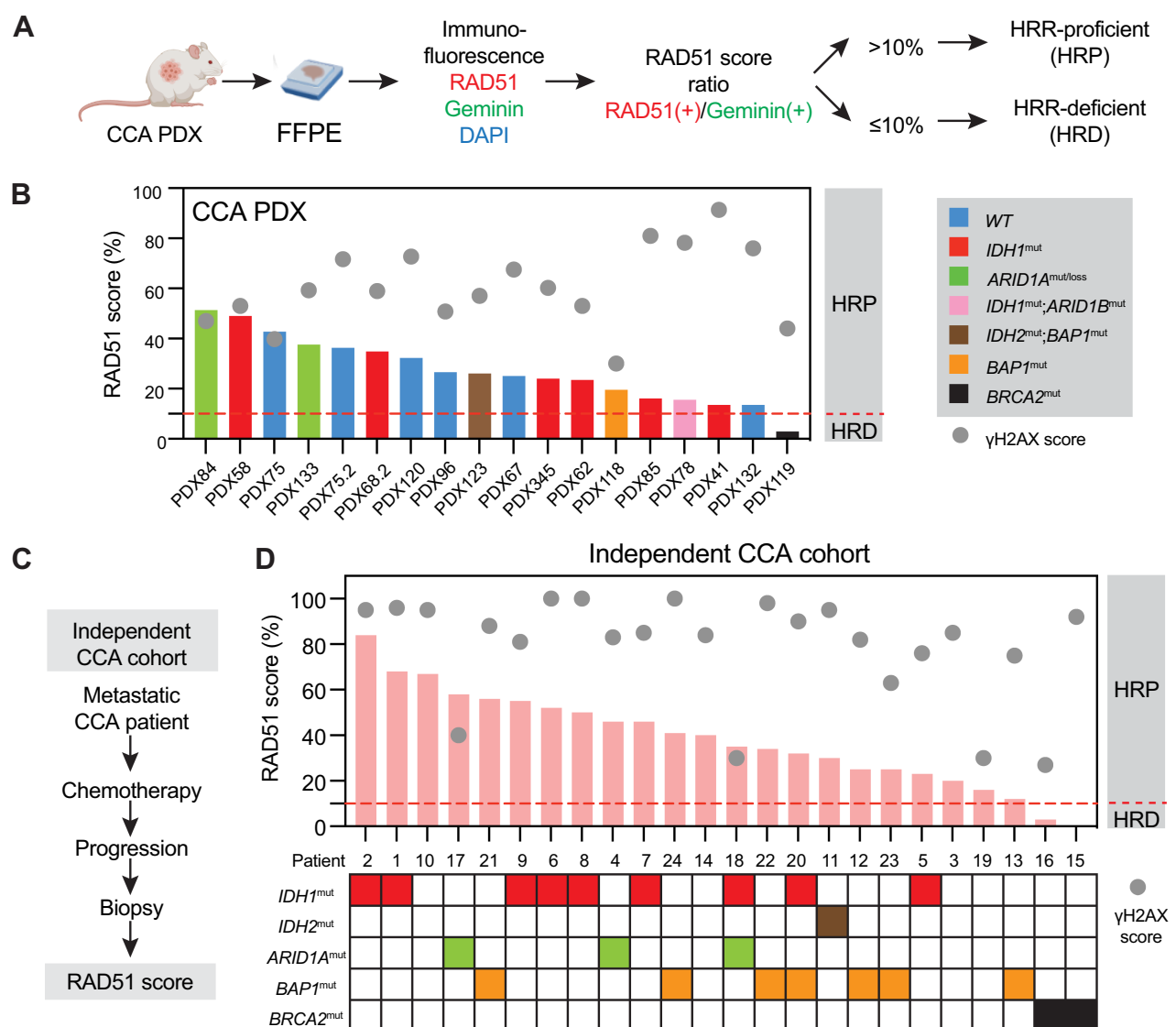
Figure 5.
RAD51 assay in CCA_PDXs and patients with CCA. **A,** Schematic illustration of the RAD51 assay and criteria used to define the proficiency or deficiency of HR repair in FFPE samples. **B,** RAD51 scores (bars) and γH2AX scores (dots) evaluated in a panel of 18 CCA_PDXs. **C,** Schematic illustration of the RAD51 assay performed in an independent CCA cohort (biopsy samples from patients with advanced CCA refractory to chemotherapy). **D,** RAD51 scores (bars) and γH2AX scores (dots) evaluated in an independent CCA cohort. Pathogenic mutations of *IDH1, IDH2, ARID1A, BAP1,* and *BRCA2* are indicated.

they are also being used for discovering cancer biomarkers and treatment (8, 49). While PDXs of CCA have been reported previously, they have mainly been established with surgically resected primary tumor tissues (11, 50–52). It is noteworthy that only approximately 25% of patients with CCA are diagnosed early and are eligible for surgical resection (1). In contrast, the remaining 75% of the CCA cases are frequently diagnosed at advanced stages with locoregional involvement or/and distant metastatic lesions, currently without long-lasting or effective therapeutic strategies (1). Despite this clear unmet clinical need, large collections of PDX models focused on unresectable advanced CCA are missing. We report here a unique collection of CCA_PDXs, of which the majority (18 of 19 CCA_PDXs) was established with biopsy samples of metastatic lesions from patients with confirmed advanced CCA disease.

This collection of CCA_PDX models faithfully recapitulates the histopathologic and genetic characteristics of the corresponding original CCA samples. Of note, the genomic profiles of the CCA_PDX collection compile a list of mutations that have been previously reported to be associated with cholangiocarcinoma pathogenesis, such as mutations in genes *TP53, KRAS, ARID1A, BAP1, BRCA2,* or *PIK3CA* (12, 13, 16, 30). Moreover, as they are established mainly from patients with metastatic intrahepatic CCA, our CCA_PDX showed a high prevalence of mutations in *IDH1/2,* which is in agreement with reported molecular traits of the intrahepatic CCA (12, 16). In addition, tumor cells derived from CCA_PDXs can grow as tumoroids using optimized *ex vivo* 3D culture conditions. Importantly, as previously reported in breast cancer (4), castration-resistant prostate cancer (32), and osteosarcoma

models (33), the drug responses observed in tumoroids derived from CCA_PDXs were in agreement with those observed with CCA_PDX and patients with CCA, thus providing a new potentially valuable platform for rapid, cheap, and high-throughput screening of drug sensitivity and resistance in CCA.

Tumor cells that lack functional BRCA1/2, key HR proteins, have been shown to be exquisitely sensitive to PARPi (47, 48). Clinical evidence demonstrated that patients with $BRCA2^{mut}$ breast, prostate, and ovarian cancers could benefit from PARPi treatment (53–55). We found that CCA-derived preclinical models with $BRCA2^{mut}$ respond to PARPi, indicating the potential application of PARPi in advanced CCA. Indeed, several recent case reports have independently documented the effectiveness of olaparib in patients with CCA with pathogenic deleterious mutations of $BRCA2$ (56–58). As $BRCA2^{mut}$ was reported in approximately 3% of patients with CCA (59), which is non-negligible, further large-scale studies are warranted to systematically evaluate the effectiveness of PARPi in these patients.

Strikingly, our $IDH1^{mut}$, $ARID1A^{mut}$, and $BAP1^{mut}$ CCA patient-derived preclinical models did not respond to PARPi treatment. Remarkably, the absence of PARPi effectiveness in these preclinical models is in contrast to what would be expected on the basis of previously published data (17–21). Interestingly, several other preclinical studies also showed a high degree of variable response of $IDH1/2^{mut}$ cancer cells to PARPis (60, 61). Moreover, a retrospective study suggested that ARID1A loss may confer PARPi resistance in patients with ovarian cancer (62). A recent phase II also reported that olaparib has limited activity in patients with previously treated mesothelioma with $BAP1$ mutations (63). Taken together, these results suggest that $IDH1^{mut}$, $ARID1A^{mut}$, and $BAP1^{mut}$ should not be used as a pan-cancer biomarker to predict PARPi response and that patients with advanced CCA with these mutations are unlikely to benefit from PARPi monotherapy. Further studies are needed to investigate in which cancer type and/or subtype these mutations are associated with sensitivity to PARPi.

To understand why our $IDH1^{mut}$, $ARID1A^{mut}$, and $BAP1^{mut}$ CCA patient-derived preclinical models did not respond to PARPi treatment, we also examined their HR status using the RAD51 assay (26, 27). Of note, this assay has been applied in several clinical trials, and tumor sample RAD51 scores can predict clinical benefits from PARPi treatment with high sensitivity and specificity (22, 24, 25). Our data showed that RAD51 scores of $IDH1^{mut}$, $ARID1A^{mut}$, and $BAP1^{mut}$ CCA_PDX, as well as those of patients with advanced CCA harboring these mutations, are compatible with an HRP profile; CCA_PDX (PDX119) and patient sample with pathogenic alterations in $BRCA2$ were, as expected, scored as HRD. Indeed, as most of our CCA_PDXs were generated from patients with advanced CCA refractory to chemotherapy, we could not exclude the possible scenario that $IDH1^{mut}$, $ARID1A^{mut}$, and $BAP1^{mut}$ CCA cells were originally deficient in HR, and that the capacity for HR was restored over the disease progression and/or course of treatment. A comparison between primary and metastatic CCA biopsy before and after the treatment could address this. We also acknowledge the limitation of having a low number of analyzed CCA patient samples in our study; further studies with RAD51 assay in larger CCA cohorts are needed to confirm our results and select patients who are likely to benefit from PARPi.

Identifying biomarkers to predict response is essential for the success of clinical trials. Accordingly, PDX models allow us to test the efficacy of new drugs both *ex vivo* and *in vivo*, and the results can help clinicians prioritize potential clinical trials and deliver precision patient care. This is especially important in tumors with an unmet clinical need, such as unresectable and advanced CCA.

Authors' Disclosures

Authors' Contributions

Q. Serra-Camprubí: Conceptualization, data curation, formal analysis, validation, investigation, visualization, writing–original draft, writing–review and editing. **H. Verdaguer:** Conceptualization, resources, data curation, formal analysis, investigation. **W. Oliveros:** Data curation, formal analysis, investigation. **N. Lupión-Garcia:** Data curation, formal analysis, investigation. **A. Llop-Guevara:** Data curation, formal analysis, investigation. **C. Molina:** Data curation, formal analysis, investigation. **M. Vila-Casadesús:** Data curation, formal analysis, investigation. **A. Turpin:** Resources, formal analysis, investigation. **C. Neuzillet:** Resources, formal analysis, investigation. **J. Frigola:** Data curation, formal analysis, investigation. **J. Querol:** Investigation. **M. Yáñez-Bartolomé:** Formal analysis, investigation. **F. Castet:** Data curation, formal analysis, investigation. **C. Fabregat-Franco:** Data curation, formal analysis, investigation. **C. Escudero-Iriarte:** Formal analysis, investigation. **M. Escorihuela:** Investigation. **E.J. Arenas:** Investigation. **C. Bernadó-Morales:** Investigation. **N. Haro:** Formal analysis, investigation. **F.J. Giles:** Resources. **Ó.J. Pozo:** Formal analysis, investigation. **J.M. Miquel:** Resources, project administration. **P.G. Nuciforo:** Resources, supervision. **A. Vivancos:** Resources, supervision. **M. Melé:** Data curation, formal analysis, supervision. **V. Serra:** Resources, supervision. **J. Arribas:** Resources, supervision. **J. Tabernero:** Resources, supervision. **S. Peiró:** Conceptualization, resources, data curation, formal analysis, supervision, funding acquisition, writing–original draft, writing–review and editing. **T. Macarulla:** Conceptualization, resources, data curation, formal analysis, supervision, funding acquisition, writing–original draft, writing–review and editing. **T.V. Tian:**

The publication costs of this article were defrayed in part by the payment of publication fees. Therefore, and solely to indicate this fact, this article is hereby marked "advertisement" in accordance with 18 USC section 1734.

Note

References

1. Banales JM, Marin JJG, Lamarca A, Rodrigues PM, Khan SA, Roberts LR, et al. Cholangiocarcinoma 2020: the next horizon in mechanisms and management. Nat Rev Gastroenterol Hepatol 2020;17:557–88.
2. Banales JM, Cardinale V, Carpino G, Marzioni M, Andersen JB, Invernizzi P, et al. Expert consensus document: Cholangiocarcinoma: current knowledge and future perspectives consensus statement from the European Network for the Study of Cholangiocarcinoma (ENS-CCA). Nat Rev Gastroenterol Hepatol 2016;13:261–80.
3. Howlader N, Noone AM, Krapcho M, Miller D, Brest A, Yu M, et al. SEER Cancer Statistics Review, 1975–2018, NCI. Bethesda, MD, https://seer.cancer.gov/csr/1975_2018/, based on November 2020 SEER data submission, posted to the SEER web site; 2021.
4. Bruna A, Rueda OM, Greenwood W, Batra AS, Callari M, Batra RN, et al. A biobank of breast cancer explants with preserved intra-tumor heterogeneity to screen anticancer compounds. Cell 2016;167:260–74.
5. DeRose YS, Wang G, Lin YC, Bernard PS, Buys SS, Ebbert MT, et al. Tumor grafts derived from women with breast cancer authentically reflect tumor pathology, growth, metastasis and disease outcomes. Nat Med 2011;17:1514–20.
6. Bertotti A, Migliardi G, Galimi F, Sassi F, Torti D, Isella C, et al. A molecularly annotated platform of patient-derived xenografts ("xenopatients") identifies HER2 as an effective therapeutic target in cetuximab-resistant colorectal cancer. Cancer Discov 2011;1:508–23.
7. Gao H, Korn JM, Ferretti S, Monahan JE, Wang Y, Singh M, et al. High-throughput screening using patient-derived tumor xenografts to predict clinical trial drug response. Nat Med 2015;21:1318–25.
8. Byrne AT, Alférez DG, Amant F, Annibali D, Arribas J, Biankin AV, et al. Interrogating open issues in cancer precision medicine with patient-derived xenografts. Nat Rev Cancer 2017;17:254–68.
9. Cho SY. Patient-derived xenografts as compatible models for precision oncology. Lab Anim Res 2020;36:14.
10. Cavalloni G, Peraldo-Neia C, Varamo C, Casorzo L, Dell'Aglio C, Bernabei P, et al. Establishment and characterization of a human intrahepatic cholangiocarcinoma cell line derived from an Italian patient. Tumour Biol 2016;37:4041–52.
11. Leiting JL, Murphy SJ, Bergquist JR, Hernandez MC, Ivanics T, Abdelrahman AM, et al. Biliary tract cancer patient-derived xenografts: surgeon impact on individualized medicine. JHEP Rep 2020;2:100068.
12. Jusakul A, Cutcutache I, Yong CH, Lim JQ, Huang MN, Padmanabhan N, et al. Whole-genome and epigenomic landscapes of etiologically distinct subtypes of cholangiocarcinoma. Cancer Discov 2017;7:1116–35.
13. Nakamura H, Arai Y, Totoki Y, Shirota T, Elzawahry A, Kato M, et al. Genomic spectra of biliary tract cancer. Nat Genet 2015;47:1003–10.
14. Nepal C, O'Rourke CJ, Oliveira D, Taranta A, Shema S, Gautam P, et al. Genomic perturbations reveal distinct regulatory networks in intrahepatic cholangiocarcinoma. Hepatology 2018;68:949–63.
15. Silverman IM, Hollebecque A, Friboulet L, Owens S, Newton RC, Zhen H, et al. Clinicogenomic analysis of FGFR2-rearranged cholangiocarcinoma identifies correlates of response and mechanisms of resistance to pemigatinib. Cancer Discov 2021;11:326–39.
16. Wardell CP, Fujita M, Yamada T, Simbolo M, Fassan M, Karlic R, et al. Genomic characterization of biliary tract cancers identifies driver genes and predisposing mutations. J Hepatol 2018;68:959–69.
17. Mateo J, Lord CJ, Serra V, Tutt A, Balmana J, Castroviejo-Bermejo M, et al. A decade of clinical development of PARP inhibitors in perspective. Ann Oncol 2019;30:1437–47.
18. Shen J, Peng Y, Wei L, Zhang W, Yang L, Lan L, et al. ARID1A deficiency impairs the DNA damage checkpoint and sensitizes cells to PARP inhibitors. Cancer Discov 2015;5:752–67.
19. Sulkowski PL, Corso CD, Robinson ND, Scanlon SE, Purshouse KR, Bai H, et al. 2-Hydroxyglutarate produced by neomorphic IDH mutations suppresses homologous recombination and induces PARP inhibitor sensitivity. Sci Transl Med 2017;9:eaal2463.
20. Sulkowski PL, Oeck S, Dow J, Economos NG, Mirfakhraie L, Liu Y, et al. Oncometabolites suppress DNA repair by disrupting local chromatin signalling. Nature 2020;582:586–91.
21. Yang H, Xu D, Gao Y, Schmid RA, Peng RW. The Association of BAP1 loss-of-function with the defect in homologous recombination repair and sensitivity to PARP-targeted therapy. J Thorac Oncol 2020;15:e88–90.
22. Guffanti F, Alvisi MF, Anastasia A, Ricci F, Chiappa M, Llop-Guevara A, et al. Basal expression of RAD51 foci predicts olaparib response in patient-derived ovarian cancer xenografts. Br J Cancer 2022;126:120–8.
23. Llop-Guevara A, Loibl S, Villacampa G, Vladimirova V, Schneeweiss A, Karn T, et al. Association of RAD51 with homologous recombination deficiency (HRD) and clinical outcomes in untreated triple-negative breast cancer (TNBC): analysis of the GeparSixto randomized clinical trial. Ann Oncol 2021;32:1590–6.
24. Carreira S, Porta N, Arce-Gallego S, Seed G, Llop-Guevara A, Bianchini D, et al. Biomarkers associating with PARP inhibitor benefit in prostate cancer in the TOPARP-B trial. Cancer Discov 2021;11:2812–27.
25. Blanc-Durand F, Yaniz E, Genestie C, Rouleau E, Berton D, Lortholary A, et al. Evaluation of a RAD51 functional assay in advanced ovarian cancer, a GINECO/GINEGEPS study. J Clin Oncol 39: 15s, 2021 (suppl; abstr; 5513).
26. Cruz C, Castroviejo-Bermejo M, Gutierrez-Enriquez S, Llop-Guevara A, Ibrahim YH, Gris-Oliver A, et al. RAD51 foci as a functional biomarker of homologous recombination repair and PARP inhibitor resistance in germline BRCA-mutated breast cancer. Ann Oncol 2018;29:1203–10.
27. Castroviejo-Bermejo M, Cruz C, Llop-Guevara A, Gutierrez-Enriquez S, Ducy M, Ibrahim YH, et al. A RAD51 assay feasible in routine tumor samples calls PARP inhibitor response beyond BRCA mutation. EMBO Mol Med 2018;10:e9172.
28. Bankhead P, Loughrey MB, Fernández JA, Dombrowski Y, McArt DG, Dunne PD, et al. QuPath: Open source software for digital pathology image analysis. Sci Rep 2017;7:16878.

29. Lau SK, Prakash S, Geller SA, Alsabeh R. Comparative immunohistochemical profile of hepatocellular carcinoma, cholangiocarcinoma, and metastatic adenocarcinoma. Hum Pathol 2002;33:1175–81.

30. Farshidfar F, Zheng S, Gingras MC, Newton Y, Shih J, Robertson AG, et al. Integrative genomic analysis of cholangiocarcinoma identifies distinct IDH-mutant molecular profiles. Cell Rep 2017;19:2878–80.

31. Hribar KC, Wheeler CJ, Bazarov A, Varshneya K, Yamada R, Buckley P, et al. A simple three-dimensional hydrogel platform enables ex vivo cell culture of patient and PDX tumors for assaying their response to clinically relevant therapies. Mol Cancer Ther 2019;18:718–25.

32. Lawrence MG, Obinata D, Sandhu S, Selth LA, Wong SQ, Porter LH, et al. Patient-derived models of abiraterone- and enzalutamide-resistant prostate cancer reveal sensitivity to ribosome-directed therapy. Eur Urol 2018;74:562–72.

33. Nomura M, Rainusso N, Lee YC, Dawson B, Coarfa C, Han R, et al. Tegavivint and the beta-catenin/ALDH axis in chemotherapy-resistant and metastatic osteosarcoma. J Natl Cancer Inst 2019;111:1216–27.

34. Fujisawa T, Filippakopoulos P. Functions of bromodomain-containing proteins and their roles in homeostasis and cancer. Nat Rev Mol Cell Biol 2017;18:246–62.

35. Fujiwara H, Tateishi K, Kato H, Nakatsuka T, Yamamoto K, Tanaka Y, et al. Isocitrate dehydrogenase 1 mutation sensitizes intrahepatic cholangiocarcinoma to the BET inhibitor JQ1. Cancer Sci 2018;109:3602–10.

36. Garcia PL, Miller AL, Gamblin TL, Council LN, Christein JD, Arnoletti JP, et al. JQ1 induces DNA damage and apoptosis, and inhibits tumor growth in a patient-derived xenograft model of cholangiocarcinoma. Mol Cancer Ther 2018;17:107–18.

37. Lu Q, Ding X, Huang T, Zhang S, Li Y, Xu L, et al. BRD4 degrader ARV-825 produces long-lasting loss of BRD4 protein and exhibits potent efficacy against cholangiocarcinoma cells. Am J Transl Res 2019;11:5728–39.

38. Shorstova T, Foulkes WD, Witcher M. Achieving clinical success with BET inhibitors as anti-cancer agents. Br J Cancer 2021;124:1478–90.

39. Morrison-Smith CD, Knox TM, Filic I, Soroko KM, Eschle BK, Wilkens MK, et al. Combined targeting of the BRD4-NUT-p300 axis in NUT midline carcinoma by dual selective bromodomain inhibitor, NEO2734. Mol Cancer Ther 2020;19:1406–14.

40. Ryan KR, Giles F, Morgan GJ. Targeting both BET and CBP/EP300 proteins with the novel dual inhibitors NEO2734 and NEO1132 leads to anti-tumor activity in multiple myeloma. Eur J Haematol 2021;106:90–9.

41. Spriano F, Gaudio E, Cascione L, Tarantelli C, Melle F, Motta G, et al. Antitumor activity of the dual BET and CBP/EP300 inhibitor NEO2734. Blood Adv 2020;4:4124–35.

42. Tian T, Cosín M, Giles F, Braña I, Garralda E, Peiró S. NEO2734, a novel dual BET and P300/CBP bromodomain inhibitor, is more active in NUT midline carcinoma than single agent BET or P300/CBP inhibitors [abstract]. In: Proceedings of the AACR-NCI-EORTC International Conference on Molecular Targets and Cancer Therapeutics; 2019 Oct 26–30; Boston, MA. Philadelphia (PA): AACR; Mol Cancer Ther 2019;18(12 Suppl):Abstract nr B008.

43. Goyal L, Saha SK, Liu LY, Siravegna G, Leshchiner I, Ahronian LG, et al. Polyclonal secondary FGFR2 mutations drive acquired resistance to FGFR inhibition in patients with FGFR2 fusion-positive cholangiocarcinoma. Cancer Discov 2017;7:252–63.

44. Goyal L, Shi L, Liu LY, Fece de la Cruz F, Lennerz JK, Raghavan S, et al. TAS-120 overcomes resistance to ATP-competitive FGFR inhibitors in patients with FGFR2 fusion-positive intrahepatic cholangiocarcinoma. Cancer Discov 2019;9:1064–79.

45. Varghese AM, Patel J, Janjigian YY, Meng F, Selcuklu SD, Iyer G, et al. Noninvasive detection of polyclonal acquired resistance to FGFR inhibition in patients with cholangiocarcinoma harboring FGFR2 alterations. JCO Precis Oncol 2021;5:PO.20.00178.

46. Heeke AL, Pishvaian MJ, Lynce F, Xiu J, Brody JR, Chen WJ, et al. Prevalence of homologous recombination-related gene mutations across multiple cancer types. JCO Precis Oncol 2018;2018:PO.17.00286.

47. Bryant HE, Schultz N, Thomas HD, Parker KM, Flower D, Lopez E, et al. Specific killing of BRCA2-deficient tumours with inhibitors of poly(ADP-ribose) polymerase. Nature 2005;434:913–7.

48. Farmer H, McCabe N, Lord CJ, Tutt AN, Johnson DA, Richardson TB, et al. Targeting the DNA repair defect in BRCA mutant cells as a therapeutic strategy. Nature 2005;434:917–21.

49. Conte N, Mason JC, Halmagyi C, Neuhauser S, Mosaku A, Yordanova G, et al. PDX Finder: a portal for patient-derived tumor xenograft model discovery. Nucleic Acids Res 2019;47:D1073–D9.

50. Cavalloni G, Peraldo-Neia C, Sassi F, Chiorino G, Sarotto I, Aglietta M, et al. Establishment of a patient-derived intrahepatic cholangiocarcinoma xenograft model with KRAS mutation. BMC Cancer 2016;16:90.

51. Gao Y, Zhou R, Huang JF, Hu B, Cheng JW, Huang XW, et al. Patient-derived xenograft models for intrahepatic cholangiocarcinoma and their application in guiding personalized medicine. Front Oncol 2021;11:704042.

52. Jiang TY, Pan YF, Wan ZH, Lin YK, Zhu B, Yuan ZG, et al. PTEN status determines chemosensitivity to proteasome inhibition in cholangiocarcinoma. Sci Transl Med 2020;12:eaay0152.

53. Robson M, Im SA, Senkus E, Xu B, Domchek SM, Masuda N, et al. Olaparib for metastatic breast cancer in patients with a germline BRCA mutation. N Engl J Med 2017;377:523–33.

54. Moore K, Colombo N, Scambia G, Kim BG, Oaknin A, Friedlander M, et al. Maintenance olaparib in patients with newly diagnosed advanced ovarian cancer. N Engl J Med 2018;379:2495–505.

55. de Bono J, Mateo J, Fizazi K, Saad F, Shore N, Sandhu S, et al. Olaparib for metastatic castration-resistant prostate cancer. N Engl J Med 2020;382:2091–102.

56. Cheng Y, Zhang J, Qin SK, Hua HQ. Treatment with olaparib monotherapy for BRCA2-mutated refractory intrahepatic cholangiocarcinoma: a case report. Onco Targets Ther 2018;11:5957–62.

57. Lin J, Shi J, Guo H, Yang X, Jiang Y, Long J, et al. Alterations in DNA damage repair genes in primary liver cancer. Clin Cancer Res 2019;25:4701–11.

58. Su YL, Ng CT, Jan YH, Hsieh YL, Wu CL, Tan KT. Remarkable response to olaparib in a patient with combined hepatocellular-cholangiocarcinoma harboring a biallelic BRCA2 mutation. Onco Targets Ther 2021;14:3895–901.

59. Spizzo G, Puccini A, Xiu J, Goldberg RM, Grothey A, Shields AF, et al. Molecular profile of BRCA-mutated biliary tract cancers. ESMO Open 2020;5:e000682.

60. Venneker S, Kruisselbrink AB, Briaire-de Bruijn IH, de Jong Y, van Wijnen AJ, Danen EHJ, et al. Inhibition of PARP sensitizes chondrosarcoma cell lines to chemo- and radiotherapy irrespective of the IDH1 or IDH2 mutation status. Cancers 2019;11:1918.

61. Higuchi F, Nagashima H, Ning J, Koerner MVA, Wakimoto H, Cahill DP. Restoration of temozolomide sensitivity by PARP inhibitors in mismatch repair deficient glioblastoma is independent of base excision repair. Clin Cancer Res 2020;26:1690–9.

62. Hu HM, Zhao X, Kaushik S, Robillard L, Barthelet A, Lin KK, et al. A quantitative chemotherapy genetic interaction map reveals factors associated with PARP inhibitor resistance. Cell Rep 2018;23:918–29.

63. Ghafoor A, Mian I, Wagner C, Mallory Y, Agra MG, Morrow B, et al. Phase 2 study of olaparib in malignant mesothelioma and correlation of efficacy with germline or somatic mutations in BAP1 gene. JTO Clin Res Rep 2021;2:100231.